Laser speckle statistics in ultrasound-modulated optical tomography

Roger Zemp, Sava Sakadžić, Chulhong Kim, Lihong V. Wang

Roger Zemp, Sava Sakadžić, Chulhong Kim, Lihong V. Wang, "Laser speckle statistics in ultrasound-modulated optical tomography," Proc. SPIE 6437, Photons Plus Ultrasound: Imaging and Sensing 2007: The Eighth Conference on Biomedical Thermoacoustics, Optoacoustics, and Acousto-optics, 64371L (27 February 2007); doi: 10.1117/12.700547

SPIE.

Event: SPIE BiOS, 2007, San Jose, California, United States

Laser speckle statistics in ultrasound-modulated optical tomography

Roger Zemp, Sava Sakadžić, Chulhong Kim, and Lihong V. Wang
Optical Imaging Laboratory, Department of Biomedical Engineering, Texas A&M University, College Station, TX, 77843-3120

ABSTRACT

Ultrasound-Modulated Optical Tomography is a novel biophotonic imaging technique that provides optical contrast with ultrasonic spatial resolution. High temporal coherence laser light and focused ultrasound are transmitted into tissue. Light passing through the acoustic focal volume experiences modulation due to acoustically induced changes in optical index of refraction and optical scatterer displacement. A component of the modulated light may be detected using various detection schemes. One such scheme detects changes in the contrast of optical speckles using a CCD camera. We use statistical optics to derive expressions for the speckle statistics as a function of acoustic parameters. We demonstrate theoretically and experimentally that low acoustic frequencies induce much larger modulation compared with high frequency ultrasound. Theoretically computed values for the speckle contrast are compared with experimental values.

Keywords: biophotonic imaging, multiply scattered light, optical speckles

1. INTRODUCTION

While imaging systems leveraging optical contrast offer great promise for medical and biological imaging, optical imaging in living subjects with high spatial resolution and significant penetration depths is challenging due to multiple scattering of light. While optical microscopy and coherence-based imaging techniques provide excellent spatial resolution, their penetration depth is fundamentally limited to length scales on the order of a transport mean-free path. Diffuse optical tomography, on the other hand, uses models of diffuse light propagation to estimate optical properties in tissue. The technique, however, relies on model assumptions, is highly ill-posed, and is conditioned upon regularization, which can blur spatial resolution with increasing imaging depths. Ultrasound-modulated Optical Tomography (UOT), aims to locally probe tissue optical properties by modulating the optical field within a spatially-confined, focused region of ultrasound. By sweeping the ultrasonic sample volume in tissue, images are formed representative of the amount of modulated light emerging from the ultrasonic sample volume, hence the images provide information about optical properties such as absorption and scattering. Theoretical contributions regarding UOT mechanisms include Leutz and Maret,[1] Mahan,[2] Lev,[3,4] Wang,[5,6] Sakadžić and Wang,[7,8] among others. Various detection systems have been devised to detect the modulated light in UOT including single square-law detectors,[9] CCD cameras,[10–13] Fabry-Perot interferometers,[14] and photo-refractive detection schemes.[15,16]

We provide a theoretical and experimental treatment of speckle contrast detection for ultrasound-modulated optical tomography, introduced for UOT in Li *et. al.*[11] There a connection between speckle contrast and modulation depth was formulated, however the theory offered no formal explanation of speckle statistics as a function of ultrasonic and optical parameters. We build on the probabilistic models of ultrasound-modulated light propagation introduced by Wang[5] and Sakadžić[6–8] to address these needs. This article presents additional supporting material to a recently published article along these lines[17] and includes experimental images of phantoms using techniques described by Kim[18] and Zemp.[19] The model provides insights into ultrasonic parameter selection for UOT experiments, and offers needed theoretic progress in understanding basic mechanisms of UOT for more future modeling efforts. Experiments validate predicted linear relationships between speckle contrast and acoustic intensity.

Photons Plus Ultrasound: Imaging and Sensing 2007: The Eighth Conference on Biomedical Thermoacoustics, Optoacoustics, and Acousto-optics, edited by Alexander A. Oraevsky, Lihong V. Wang,
Proc. of SPIE Vol. 6437, 64371L, (2007) · 1605-7422/07/$18 · doi: 10.1117/12.700547

2. THEORY

2.1. Speckle Statistics as a Function of Optical and Ultrasonic Parameters

We consider the propagation of infinitely-long coherence-length laser light through a homogeneous optically scattering medium with discrete optical scatterers insonified by a monochromatic ultrasound plane wave. The intensity $I_p(t)$ of one speckle spot as a function of time can be given as the intensity of electric field due to a sum of many scattered wave components. The electric field (neglecting polarization) on a detector element p of the detector array may be written as:

$$E_p(t) = \left(\sum_{i=1}^{N_p} E_i(t) \right), \tag{1}$$

and the intensity as

$$I_p(t) = |E_p(t)|^2 \tag{2}$$

where the expressions are evaluated for a single realization of a scatterer distribution Ξ. Here $E_i(t)$ is the complex electric field contribution of the ith partial wave due to a given scattered light path. N_p is the number of partial waves originating from N_p photon paths.

2.1.1. First Order Statistics of CCD Pixel Intensities

The time-averaged intensity of one speckle spot is given as $\overline{I_p} = \langle I_p(t) \rangle_t$. We assume that the CCD exposure times T are much longer than optical and ultrasonic periods such that we can safely assume that $\langle I_p(t) \rangle_t = \lim_{T \to \infty} \frac{1}{T} \int_0^T I_p(t) dt$. The mean intensity averaged over pixels p of the CCD is given as:

$$\langle \overline{I_p} \rangle_p \approx \langle \overline{I_p} \rangle_\Xi = \left\langle E_p(t) E_p^*(t) \right\rangle_{\Xi,t}. \tag{3}$$

Here the middle equality follows from an assumption of spatial ergodicity,[20] that is, we assume that the first and second-order speckle statistics are not spatially varying.

We also assume that the photon mean free path is much longer than the optical wavelength (weak scattering approximation) and the acoustic particle displacements are much less than the optical wavelength.

With these conditions in mind, Eq. (3) is evaluated as:

$$\langle \overline{I_p} \rangle_p \approx G_1(0) = I_0, \tag{4}$$

where I_0 is the mean optical intensity. Here

$$G_1(\tau) = \langle \Gamma_1(t, \tau) \rangle_t \tag{5}$$

is the time-average of the temporal field autocorrelation function[5,7]

$$\Gamma_1(t, \tau) = \langle E_p(t) E_p^*(t + \tau) \rangle_\Xi \tag{6}$$

2.1.2. Second Order Statistics of CCD Pixel Intensities

We want to compute the variance of the speckle pattern on the CCD surface. We again rely on spatial ergodicity to compute the second-order moment of intensity:

$$\begin{aligned} \langle \overline{I_p}^2 \rangle_p &\approx \langle \overline{I_p}^2 \rangle_\Xi \\ &= \langle \langle E_p(t) E_p^*(t) \rangle_t \langle E_p(t') E_p^*(t') \rangle_{t'} \rangle_\Xi \\ &= \langle \langle E_p(t) E_p^*(t) E_p(t') E_p^*(t') \rangle_\Xi \rangle_{t,t'}. \end{aligned} \tag{7}$$

When we make the substitution $t' = t + \tau$, this is recognized as $\langle G_2(\tau) \rangle_\tau$, where

$$G_2(\tau) = \langle I_p(t) I_p(t + \tau) \rangle_{\Xi,t} \tag{8}$$

is the time-averaged temporal intensity autocorrelation function.

2.1.3. Circular Gaussian Electric Field Statistics

We note from Eq. (1) that the complex electric field E_p is composed of a large number of statistically independent zero-mean random processes, E_i. Using the *Central Limit Theorem*,[20] $E_p(t)$ is well modelled by a zero-mean complex *Normal* process with approximately uniformly distributed phase (a circular Gaussian distribution). The instantaneous intensity is thus well represented by a Rayleigh distribution. The intensity statistics over CCD pixels may be more complicated than Rayleigh, or even Rician due to temporal and spatial integration occuring in the detection process.

2.1.4. Fourth Order Moments of the Electric Field Stocahstic Process

With normally distributed electric field statistics we now use a fourth-order moment theorem for normal stochastic processes[21] to write

$$\begin{aligned} &\langle E_p(t)E_p^*(t)E_p(t+\tau)E_p^*(t+\tau)\rangle_\Xi \\ &= \langle E_p(t)E_p^*(t)\rangle_\Xi\langle E_p(t+\tau)E_p^*(t+\tau)\rangle_\Xi \\ &+\langle E_p(t)E_p(t+\tau)\rangle_\Xi\langle E_p^*(t)E_p^*(t+\tau)\rangle_\Xi \\ &+\langle E_p(t)E_p^*(t+\tau)\rangle_\Xi\langle E_p^*(t)E_p(t+\tau)\rangle_\Xi, \end{aligned} \tag{9}$$

thus expressing expectation into a sum of products of second order moment contributions. The second term on the right-hand side of Eq. (9) vanishes due to ensemble averaging over uniformly distributed phase. Using Eq. (14), the second moment of speckle intensity, Eq. (7), can be written as

$$\langle G_2(\tau)\rangle_\tau = G_1^2(0) + \langle|\Gamma_1(t,\tau)|^2\rangle_{t,\tau} \tag{10}$$

and the speckle variance is the second moment, less the square of the mean:

$$\sigma^2 = \langle|\Gamma_1(t,\tau)|^2\rangle_{t,\tau}. \tag{11}$$

2.2. Contrast of Speckles

Speckle contrast is defined as the ratio of the standard deviation and mean of speckle intensity measurements over the CCD:

$$C = \frac{\sigma}{\langle\overline{I}_s\rangle_p}. \tag{12}$$

Inserting calculated values for mean and standard deviation of speckle intensity, we have

$$C = \frac{\sqrt{\langle|\Gamma_1(t,\tau)|^2\rangle_{t,\tau}}}{G_1(0)} \tag{13}$$

2.3. Path Integral Evaluation of the Electric Field Autocorrelation Function

We are now in a position to connect with previously derived approximations for the autocorrelation, which will allow us to connect observations of speckle contrast to acoustic and optical parameters.

$$\begin{aligned} \Gamma_1(t,\tau) &= \langle E_p(t)E_p^*(t+\tau)\rangle_\Xi \\ &= \sum_{i=1}^{N_p}\sum_{j=1}^{N_p}\langle E_i(t)E_j^*(t+\tau)\rangle_\Xi \\ &= \sum_{i=1}^{N_p}\langle E_i(t)E_i^*(t+\tau)\rangle_\Xi \\ &= \int_0^\infty p(s)\langle E_s(t)E_s^*(t+\tau)\rangle_H ds. \end{aligned} \tag{14}$$

In Eq. (14) we follow the diffusing-wave spectroscopy approach,[22,23] where it is assumed that in the weak scattering approximation the correlation between different random paths vanishes and only the photons traveling along the same physical path (meaning a given sequence of scatterers) produce a nonzero effect. $E_s(t)$ is the electric field from paths of length s and $p(s)$ is the probability density function of s. H is the space of all possible realizations of paths of pathlength s (discussed more precisely by Sakadžić[7,8]). Because s is related to photon propagation times, in the diffusion regime, $p(s)$ can be modeled by time-resolved diffusion-theoretic approaches.[24] Our assumptions of spatial ergodicity rely on the fact that the CCD detector is sufficiently far from the sample that the modulated diffuse light produces a fairly uniform speckle field over the CCD surface. In Eq. (14) we neglect Brownian motion or assume that the CCD integration time is sufficiently brief so as to ignore Brownian motion induced speckle decorrelation.

With the autocorrelation expressed as an integral over optical paths, we can write (14) as:

$$\Gamma_1(t,\tau) = I_0 \int_0^\infty p(s)\langle \exp(-i\Delta\varphi_s(t,\tau))\rangle_H ds, \tag{15}$$

where $\Delta\varphi(t,\tau)$ is the difference of accumulated phase due to ultrasound modulation mechanisms at two time moments along the same path, which we assume is small for small ultrasonic pressures, and for further conditions discussed in Ref.[8] The accumulated phase increments are given as:

$$\Delta\varphi_s(t,\tau) = \sum_{j=1}^{N} \Delta\varphi_{n,j}(t,\tau) + \sum_{j=1}^{N} \Delta\varphi_{d,j}(t,\tau) \tag{16}$$

Here there are two types of phase increments: $\Delta\varphi_{n,j}(t,\tau)$ the phase variation induced by the modulated index of refraction along the jth free path. Also $\Delta\varphi_{d,j}(t,\tau)$ is the phase variation induced by the modulated displacement of the jth scatterer following the jth free path. Summation is going over all N free paths and $N-1$ scattering events along the photon path. Expressions for $\Delta\varphi_{s,n}(t,\tau) \equiv \sum_{j=1}^{N} \Delta\varphi_{n,j}(t,\tau)$ and $\Delta\varphi_{s,d}(t,\tau) \equiv \sum_{j=1}^{N} \Delta\varphi_{d,j}(t,\tau)$ are obtained from Eq. 19 of Sakadžić[8] by assuming $n = 1$, meaning a monochromatic ultrasound field:

$$\begin{aligned} \Delta\varphi_{s,n} &= -\frac{\Lambda}{4k_a}\eta \exp(i\omega_a t)\left[\exp(i\omega_a \tau) - 1\right] \\ &\times \sum_{j=0}^{N} \frac{1}{\chi_{j+1}}\left[\exp(-ik_a x_{j+1}) - \exp(-ik_a x_j)\right] \end{aligned} \tag{17}$$

$$\begin{aligned} \Delta\varphi_{s,n} &= -\frac{\Lambda}{4k_a} S \exp(i\omega_a t - i\phi)\left[\exp(i\omega_a \tau) - 1\right] \\ &\times \sum_{j=1}^{N} (\chi_j - \chi_{j+1}) \exp(-ik_a x_j) \end{aligned} \tag{18}$$

Here $\Lambda = 2n_0 k_0 P_0/(\rho v_a^2)$ where n_0 is the index of refraction, $k_0 = 2\pi/\lambda_0$ is the magnitude of the optical wavevector, P_0 is the ultrasound pressure, ρ is the mass density of the medium, and v_a is the ultrasound velocity. k_a is the ultrasonic wavevector magnitude, ω_a is the ultrasonic angular frequency, η is the elasto-optic coefficient, approximately equal to 0.32 in water at standard conditions. Also, χ_{j+1} is the cosine of the angle between the ultrasound wavevector $\vec{k}_a$ and the vector $\vec{l}_{j+1} = \vec{r}_{j+1} - \vec{r}_j$ which connects two different scatterers. x_j is the component of the scatterer position vector $\vec{r}_j$ in the ultrasonic wavevector direction. The multivariate process H represents the set of random variables $\{\vec{r}_0, \chi_1, l_1, ..., \chi_{N+1}, l_{N+1}\}$ associated with the paths of length s with N scatterers. S and ϕ are the relative amplitude and phase of the mean particle displacement relative to the fluid displacement, which we can assume for CW ultrasound and small particle sizes are close to 1 and 0 respectively.

At this point we may use a Taylor expansion on the exponential term in Eq. 15. First-order terms average to zero, and terms higher than second order are neglected. Consequently, to the second order,

$$\langle|\Gamma_1(t,\tau)|^2\rangle_{t,\tau} = I_0^2\left(1-\int_0^\infty p(s)\langle\Delta\varphi_s^2(t,\tau)\rangle_{H,t,\tau}ds\right). \tag{19}$$

Now our problem reduces to evaluating $\langle\Delta\varphi_s^2(t,\tau)\rangle_{H,t,\tau}$. The difference of accumulated phase

$$\Delta\varphi_s(t,\tau) = \Delta\varphi_{s,n}(t,\tau) + \Delta\varphi_{s,d}(t,\tau), \tag{20}$$

is due to two physical mechanisms: ultrasound-induced optical scatterer displacement and ultrasound-induced changes in the optical refractive index of the medium, represented by the first and second terms on the right-hand side of Eq. (20) respectively.

The evaluation of the second-order moment of $\Delta\varphi_s$:

$$\begin{aligned}\langle\Delta\varphi_s^2(t,\tau)\rangle_{H,t} &= \langle\Delta\varphi_{s,n}^2\rangle_{H,t} + \langle\Delta\varphi_{s,d}^2\rangle_{H,t} \\ &+ \langle 2\Delta\varphi_{s,n}\Delta\varphi_{s,d}\rangle_{H,t}\end{aligned} \tag{21}$$

was calculated in Eq. (29) of Sakadžić and Wang,[8] assuming isotropic scattering, where $\langle\Delta\varphi_{s,n}^2\rangle_{H,t}$, $\langle\Delta\varphi_{s,d}^2\rangle_{H,t}$, and $\langle\Delta\varphi_{s,n}\Delta\varphi_{s,d}\rangle_{H,t}$ are the auto- and cross-correlations of accumulated optical phase differences due to ultrasound-induced optical refractive index changes and time-varying optical scatterer displacements. Averaging over τ gives our desired results:

$$\langle\Delta\varphi^2(t,\tau)\rangle_{H,t,\tau} = \frac{1}{2}\left(C_n + C_d + C_{n,d}\right) \tag{22}$$

where C_n, C_d, and $C_{n,d}$ are given by Eq. (30) of Sakadžić:[8]

$$\begin{aligned}C_n &= \Lambda^2\frac{\eta^2}{k_a^2}(k_a l)^2\left[\left(\frac{s}{l}+1\right)\frac{G}{1-G} - \frac{G^2(1-G^{s/l+1})}{(1-G)^2}\right], \\ C_d &= \Lambda^2\frac{S^2}{k_a^2}\left[\frac{s}{3l} - \frac{1-G^{s/l-1}}{(k_a l)^2}\right], \\ C_{n,d} &= \Lambda^2\frac{2\eta S\cos(\phi)}{k_a^2}\left[-\frac{s}{l} + \frac{G(1-G^{s/l})}{1-G}\right].\end{aligned} \tag{23}$$

In Eq. (23), $G = (k_a l)^{-1}\arctan(k_a l)$, where l is the isotropic mean-free path. Anisotropic scattering can be considered by replacing l with the transport mean-free path $l_{tr} = l/(1-g)$ (where g is the scattering anisotropy factor) in the above equations, by virtue of a similarity relation.

2.4. Contrast of Speckles Related to Acoustic Parameters

Inserting calculated values for mean and standard deviation of speckle intensity into the expression for speckle contrast, we have

$$\begin{aligned}C &= \frac{\sqrt{\langle|\Gamma_1(t,\tau)|^2\rangle_{t,\tau}}}{G_1^2(0)} \\ &\approx 1 - \frac{1}{2}\int_0^\infty p(s)\langle\Delta\varphi_s^2(t,\tau)\rangle_{H,t,\tau}ds,\end{aligned} \tag{24}$$

where the last expression keeps only first order terms (in $\langle\Delta\varphi_s^2(t,\tau)\rangle_{H,t,\tau}$). The difference in speckle contrast ΔC between ultrasound off and ultrasound on states is then evaluated as:

$$\Delta C = \frac{1}{2}\int_0^\infty p(s)\left(C_n + C_d + C_{n,d}\right)ds. \tag{25}$$

Since all the C-terms of Eq. (23) are proportional to P_0^2 we note that ΔC is proportional to acoustic intensity.

2.4.1. High Ultrasound Frequencies

If we consider ultrasound frequencies f_a high enough that $k_a l_{tr}$ is much larger than 1, G tends to $\pi/(2k_a l_{tr})$. Also, as our framework is derived for the diffusion regime, we should consider optical scattering paths much longer than the transport mean-free path. In this case $C_n + C_d + C_{n,d} \approx C_n$ which is approximately $\Lambda^2 \frac{\eta^2}{k_a^2}(k_a l_{tr})^2 G \frac{s}{l_{tr}}$, and the change in speckle contrast between ultrasound on and ultrasound off states, ΔC, is given as

$$\Delta C \approx \frac{\bar{s}}{4}\left(n_0 k_0 \frac{P_0}{\rho v_a^2}\right)^2 \eta^2 \frac{v_a}{f_a}. \tag{26}$$

The term $\bar{s} \equiv \int_0^\infty sp(s)ds$ reflects the mean pathlength for a given light-propagation geometry.

2.5. Speckle Contrast Connection with Modulation Depth

Modulation depth, M, defined as the ratio of modulated light intensity $\langle I_m \rangle$ to unmodulated light intensity $\langle I_b \rangle$ is directly related to the change in speckle contrast ΔC between ultrasound on and ultrasound off states as we now show. It was previously shown by Li *et. al.*[11] that the intensity of light on a CCD pixel as a function of time t can be modelled as:

$$I = I_b + I_m + 2(I_b I_m)^{1/2} cos(\omega_a t + \Delta\phi) \tag{27}$$

where I_b and I_m are the intensities of the unmodulated and modulated light respectively, ω_a is the acoustic angular frequency, and $\Delta\phi$ is the phase difference between the modulated and unmodulated light. Assuming that the CCD integration time is large compared to an ultrasonic period, it was shown that the ultrasound-on speckle contrast can be modeled as:

$$C \approx \frac{C_b}{1+M} \tag{28}$$

where C_b is the speckle contrast due to the unmodulated light with no ultrasound. For small modulation depths, the change in speckle contrast can be written as

$$\Delta C \approx C_b M. \tag{29}$$

This suggests that for small accumulated phase differences, the change in speckle contrast ΔC is directly proportional to the modulation depth, and that the modulation depth can be related to acoustic and optical parameters via the equations derived in this article.

3. EXPERIMENT

Our experimental setup is illustrated in Fig. 1. We used a long coherence-length Nd:YAG (Coherent, Verdi; 532-nm wavelengths), and 1-MHz (Ultran VHP100-1-138: with 38-mm focal length) and 3.5 MHz (Panametrics V380: with 49-mm focal length) transducers. Both transducers had a 25 mm diameter active aperture. To acquire one point of an image we apply ultrasonic bursts while using a CCD camera to detect modulated light originating from the ultrasonic sample volume.

Light emerging from the sample was collected by a digital CCD camera (Basler, A312f; 12-bit, 640×480) with an attached tube with an appropriate length-diameter ratio to match the average speckle spot size with to the CCD pixel size. A function generator (Agilent, 33250A) synthesized 2 ms bursts that were subsequently amplified by an RF power amplifier (ENI, Inc., 325LA) to drive the ultrasound transducer. Burst initiation triggered a pulse-delay generator (Stanford Research, DG535) that produced two CCD trigger pulses for each burst. One image was captured with ultrasound on while the subsequent image was acquired with ultrasound off. Our phantom was constructed from homogeneous 10% gelatin, 10% cornstarch phantom in a 2-cm thick slab geometry with reduced scattering coefficient $\mu_s' = 9.2$ cm^{-1} as measured by the Oblique-Incidence Diffuse Reflectance technique.[25]

To experimentally investigate the theoretical prediction that laser speckle contrast decreases linearly with acoustic intensity we measure speckle contrast with both 1-MHz and 3.5-MHz transducers. Fig. 2 of Zemp *et. al.*[17] shows $|\Delta C|$, between ultrasound-off and ultrasound-on as a function of time-averaged acoustic intensity. 50 pairs of on-off speckle contrast measurements were used to estimate each data point and errorbars are smaller than data marker sizes. The spatial peak time-averaged acoustic intensity is defined as $I_{spta} = P_0^2/(2\rho v_a)$ where P_0 is the peak acoustic pressure, ρ is the mass density of the sample, and v_a is the speed of sound.

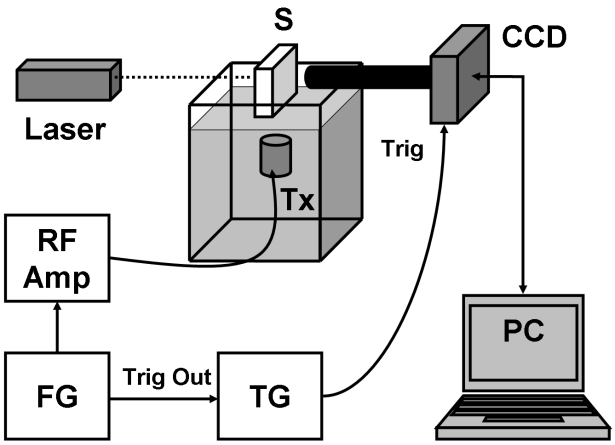

Figure 1. Experimental setup. S, Sample; CCD, CCD camera; AMP, RF amplifier; FG, Function generator; TG, Trigger generator; Tx, Ultrasound transducer.

3.1. Imaging

Fig. 2 shows a short-exposure burst-synchronized 2-D image obtained without any averaging (i.e. one acoustic burst per image pixel). The phantom is a 20-mm-thick gelatin-cornstarch sample containing two Trypan-Blue dyed objects (separated by 12 mm, from center to center). The sizes of the two objects were approximately 2 mm × 1.5 mm × 15 mm and 2.5 mm × 1.7 mm × 15 mm along the X, Y, and Z axes. In the image, the objects are clearly seen (Fig. 8). We used 1.5 MPa bursts of duration 0.2 ms. The CCD camera synchronized with these bursts used an exposure time of 0.2 ms.

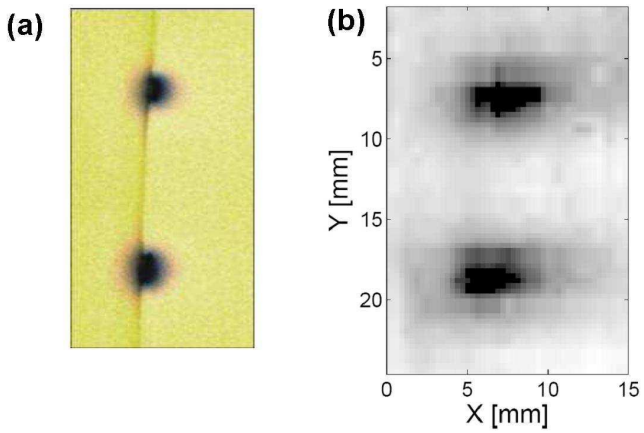

Figure 2. (a) photograph of a cross section from an optically-scattering gelatin phantom with 2 dyed objects. (b) The corresponding 2-D UOT image of the phantom. No averaging was used (i.e. one acoustic burst per image pixel). We used intense 0.2ms-duration 1.5 MPa bursts and CCD exposure time synchronized with the burst period.

4. DISCUSSION

As predicted, Fig. 2 of Zemp[17] shows linear growth of the change in speckle contrast with acoustic intensity for both 1- and 3.5-MHz transducers as evidenced by the high linear correlation coefficients 0.9995 and 0.9978

respectively. The experimental results agree with the theoretical prediction of linearity with intensity even though the theoretical model did not account for spatially varying acoustic fields.

Of significant note for maximizing signal-to-noise in a UOT system, the 1 MHz transducer offers considerably more signal than the 3.5 MHz transducer. The ratio of slopes between 1 and 3.5 MHz in Fig. 2 of Zemp[17] is approximately 18:1. We use Eq. (26) as a rough estimate to compute an expected slope ratio to compare with experiments. In doing so, we realize that we do not have a plane acoustic wave as assumed by theory, however, we approximate the principal light-ultrasound interaction region as plane-wave homogeneous over a bounded volume representative of the ultrasonic focal zone. For 1 MHz, the mean photon pathlength $\bar{s}$ should be greater than the focal beam width of 2.3 mm and for 3.5 MHz $\bar{s}$ is close to the ultrasound beam focal width of 0.85 mm. In making estimates of the predicted slope ratios, we should note that the assumptions needed to make the theory analytically tractable do not closely match the experimental conditions. In particular: (1) the focal widths are likely too small to accurately use the diffusion-approximation for light transport across the light-ultrasound interaction region (2) the acoustic field is spatially inhomogeneous rather than a plane wave (3) $k_a l_{tr}$ for 1 MHz is not much larger than 1 thus reducing the accuracy of Eq. (26) (4) optical index of refraction changes due to pressures greater than 10^5 Pa may be large enough to bend photon paths in a way not presently accounted for by theory (5) the theory does not account for polarization, Brownian motion, or imperfect temporal coherence of the laser source, effects that may tend to blur speckle contrast over the CCD exposure period. Indeed we note that the maximum ultrasound-off speckle contrast C_{max} experimentally observed is $\sim$0.3 rather than 1.

Note that the amount of unmodulated light passing around the acoustic focal zone will affect ΔC. Equations for ΔC such as Eq. (26) may be modified to include a multiplicative factor ζ representing the fraction of light passing through the ultrasonic focal zone (see endnote *). We estimate the fraction of light passing through the beam focal region as $\zeta_{1MHz} \sim 0.3$ and $\zeta_{3.5MHz} \sim 0.1$ †.

Accounting for ζ, and the other factors discussed above, Eq. 26 predicts that the slope ratio should be $\sim$28:1. This very rough estimate differs from the measured slope ratio by approximately 50%. Using $C_{max} = 0.3$, the absolute values of the slopes for 1 and 3.5 MHz are estimated within an order of magnitude of the measured values of 0.0037 cm^2/W and 0.0002 cm^2/W, respectively. Since our theoretical assumptions do not closely match the experimental conditions, the order-of magnitude agreement is as much as we can expect. Future work should address spatially varying acoustic fields and modulated light transport across sub-diffusion-regime sample volumes.

5. CONCLUSIONS

A statistical optics approach of speckle in ultrasound-modulated optical tomography has lead to the prediction that speckle contrast will change linearly with acoustic intensity - a prediction which was validated experimentally. Significantly more modulated light produced with 1-MHz ultrasound as compared with 3.5-MHz ultrasound, due to a larger acoustic focal volume, larger ultrasound-induced particle displacement, and enhanced optical field modulation due to index-of-refraction mechanisms. UOT images of phantoms were produced with 1 MHz ultrasound, requiring only one acoustic pulse per image pixel.

6. ACKNOWLEDGEMENTS

We gratefully acknowledge funding from the National Institutes of Health, R33 CA 094267.

*This is justified by modifying Eq. 15 as $\Gamma_1(t,\tau) = I_0\{(1-\zeta) + \zeta \int_0^\infty p(s)\langle \exp(-i\Delta\varphi_s(t,\tau))\rangle_H ds\}$ where $1-\zeta$ is the fraction of light passing around the acoustic sample volume. Continuing the derivations produces a modified Eq. (24) given as $\Delta C = 1 - \frac{1}{2}\zeta \int_0^\infty p(s)\langle \Delta\varphi_s^2(t,\tau)\rangle_{H,t,\tau} ds$.

†We assumed a 10 mm diffuse light pattern at the focal zone depth of 10 mm below the phantom, and estimate the area of the beam-waist in this zone as a fraction of the total illumination area. For example, for 1 MHz, we estimate $\zeta = 2.3\text{mm} \times 10\text{mm}/[\pi(5\text{mm})^2]$.

REFERENCES

1. W. Leutz and G. Maret, "Ultrasonic modulation of multiply scattered coherent light," *Physica B* **204**, pp. 14–19, 1995.
2. G. D. Mahan, W. E. Engler, J. J. Tiemann, and E. G. Uzgiris *Proc. Natl. Acad. Sci. USA* **95**, pp. 14015–14019, 1998.
3. A. Lev and B. G. Sfez, "Direct, noninvasive detection of photon density in turbid media," *Opt. Lett.* **27**(7), pp. 473–475, 2002.
4. A. Lev and B. Sfez, "In vivo demonstration of the ultrasound-modulated light technique," *J. Opt. Soc. Am. A* **20**(12), pp. 2347–2354, 2003.
5. L. H. Wang, "Mechanisms of ultrasonic modulation of multiply scattered coherent light: an analytic model," *Physical Review Letters* **87**, pp. 043903–(14), 2001.
6. L. H. Wang, "Mechanisms of ultrasonic modulation of multiply scattered coherent light: a monte carlo model," *Optics Letters* **26**, p. 11911193, 2001.
7. S. Sakadžić and L. H. Wang, "Ultrasonic modulation of multiply scattered coherent light: an analytical model for anisotropically scattering media," *Physical Review E* **66**(2), pp. 1–9, 2002.
8. S. Sakadžić and L. H. Wang, "Modulation of multiply scattered coherent light by ultrasonic pulses: An analytic model," *Physical Review E* **72**, pp. 036620–1–12, 2005.
9. L. H. Wang, S. L. Jacques, and X. Zhao, "Continuous-wave ultrasonic modulation of scattered laser light to image objects in turbid media," *Opt. Lett.* **20**, pp. 629–631, 1995.
10. S. Leveque, A. C. Boccara, M. Lebec, and H. Saint-Jalmes, "Ultrasonic tagging of photon paths in scattering media: parallel speckle modulation processing," *Opt. Lett.* **24**, pp. 181–183, 1999.
11. J. Li, G. Ku, and L. H. Wang, "Ultrasound-modulated optical tomography of biological tissue using contrast of laser speckles," *Applied Optics* **41**(28), pp. 6030–6035, 2005.
12. M. Kempe, M. Larionov, D. Zaslavsky, and A. Z. Genack, "Acousto-optic tomography with multiple scattered light," *J. Opt. Soc. Am.* **14**, pp. 1151–1158, 1997.
13. J. Li and L. H. Wang, "Methods for parallel-detection-based ultrasound-modulated optical tomography," *Applied Optics* **41**(10), pp. 2079–2084, 2002.
14. S. Sakadžić and L. H. Wang, "High-resolution ultrasound-modulated optical tomography in biological tissues," *Optics Letters* **29**(23), pp. 2770–2772, 2004.
15. F. Ramaz, B. C. Forget, M. Atlan, and A. C. Boccara, "Photorefractive detection of tagged photons in ultrasound modulated optical tomography of thick biological tissues," *Optics Express* **12**(22), pp. 5469–5474, 2004.
16. T. W. Murray, L. Sui, G. Maguluri, R. A. Roy, A. Nieva, F. Blonigen, and C. A. DiMarzio, "Detection of ultrasound-modulated photons in diffuse media using the photo-refractive effect," *Optics Letters* **29**(21), pp. 2509–2511, 2004.
17. R. J. Zemp, S. Sakadžić, and L. H. Wang, "Stochastic explanation of speckle contrast detection in ultrasound-modulated optical tomography," *Phys. Rev. E* **73**(6, Pt. 1).
18. C. H. Kim, R. J. Zemp, and L. H. Wang, "Transient acoustic radiation force as a signal enhancement mechanism in ultrasound-modulated optical tomography," *Optics Letters* , Submitted 2005.
19. R. J. Zemp, C. H. Kim, and L. V. Wang, "Ultrasound-modulated optical tomography with intense acoustic bursts," *Accepted for publication in Applied Optics* , 2006.
20. A. Papoulis and S. U. Pillai, *Probability, Random Variables and Stochastic Processes, 4th Ed.*, McGraw-Hill, New York, 2002.
21. D. Middleton, *An Introduction to Statistical Communication Theory*, Penninsula Publishing, Los Altos, CA, 1987.
22. G. Maret and P. E. Wolf *Z. Phys. B.* **65**, p. 409, 1987.
23. D. J. Pine, D. A. Weitz, P. M. Chaikin, and E. Herbolzheimer *Phys. Rev. Lett.* **60**, p. 1134, 1988.
24. M. S. Patterson, B. Chance, and B. C. Willson *Applied Optics* **28**, p. 2331, 1989.
25. G. Marquez and L. H. Wang, "White light oblique incidence reflectometer for measuring absorption and reduced scattering spectra of tissue-like turbid media," *Optics Express* **1**, pp. 454–460, 1997.